ppGpp is a bacterial cell size regulator

Ferhat Büke[1,2], Jacopo Grilli[3], Marco Cosentino Lagomarsino[4,5], Gregory Bokinsky[1]*, Sander J. Tans[1,2]*

(1) Department of Bionanoscience, Kavli Institute of Nanoscience, Delft University of Technology, Delft, The Netherlands

(2) AMOLF, Amsterdam, The Netherlands.

(3) The Abdus Salam International Centre for Theoretical Physics (ICTP), Strada Costiera 11, 34014 Trieste, Italy

(4) IFOM, FIRC Institute of Molecular Oncology, Via Adamello 16, 20143, Milan, Italy

(5) Physics Department, University of Milan, and I.N.F.N., Via Celoria 16, 20133, Milan, Italy

*Corresponding authors. These authors contributed equally to the manuscript.

Email: s.tans@amolf.nl; g.e.bokinsky@tudelft.nl

Summary

Growth and division are central to cell size. Bacteria achieve size homeostasis by dividing when growth has added a constant size since birth, termed the adder principle, by unknown mechanisms [1, 2]. Growth is well known to be regulated by ppGpp, which controls diverse processes from ribosome production to metabolic enzyme activity and replication initiation, and whose absence or excess can induce stress, filamentation, and small growth-arrested cells [3-6]. These observations raise unresolved questions about the relation between ppGpp and size homeostasis mechanisms during normal exponential growth. Here, to untangle effects of ppGpp and nutrients, we gained control of cellular ppGpp by inducing the synthesis and hydrolysis enzymes RelA and Mesh1. We found that ppGpp not only exerts control over the growth rate, but also over cell division and hence the steady state cell size. In response to changes in ppGpp level, the added size already establishes its new constant value while the growth rate still adjusts, aided by accelerated or delayed divisions. Moreover, the magnitude of the added size and resulting steady-state birth size correlate consistently with the ppGpp level, rather than with the growth rate, which results in cells of different size that grow equally fast. Our findings suggest that ppGpp serves as a key regulator that coordinates cell size and growth control.

Keywords: ppGpp; cell size; growth rate; cell size homeostasis; adder mechanism; Escherichia coli; microfluidics; microscopy; single cell analysis; lineage tree analysis.

Results

Bacterial cell size and growth coordination

Many bacterial species are known to display faster average growth and larger cell sizes in nutrient-rich media – a correlation that is also referred to as the growth law [7-9]. Yet, how cells coordinate size and growth is understood only partially. During the cell cycle, individual cells are found to grow until a constant volume is added on average, and then divide. This adder principle is observed across diverse domains of life, and can explain how the mean cell size remains constant in fixed conditions – despite random variations in cellular size at birth, and the stochastic and exponential nature of growth [1, 2, 10]. While the molecular basis remains unresolved, mechanisms for the adder behavior have been proposed that are based on DNA replication initiation [11-14], replication initiation and cell division [15], cellular surface to volume ratio [16], and the accumulation of division proteins [17]. In *Escherichia coli*, the signaling molecule guanosine tetraphosphate (ppGpp) is well-known to be a key regulator of cellular growth [18]. The ppGpp concentration is inversely proportional to the exponential growth rate and accumulates to extreme levels during amino acid deprivation (a phenomenon specifically known as the stringent response) as well as during many other stress conditions [6, 19-24]. ppGpp regulates the transcription of ribosomal RNA as well as other genes, and is reported to allosterically control metabolic enzymes [25, 26] and chromosome replication initiation [27]. However, despite the importance of growth in cellular size control, the role of ppGpp in size regulation mechanisms including the adder principle remains poorly understood.

Control of ppGpp synthesis and hydrolysis

To study the relation between ppGpp, cell growth and division, and to disentangle it from metabolic limitation effects, two enzymes were used: the catalytic domain of the *E. coli* (p)ppGpp synthesis enzyme RelA (known as RelA') [6, 28, 29] fused to YFP, creating RelA'-YFP (here referred to as RelA*), and the *Drosophila melanogaster* ppGpp hydrolysis enzyme Mesh1 [30, 31] fused to CFP (fusion here referred to as Mesh1*), inducible by dox and IPTG, respectively (Fig. 1A). As pppGpp produced by RelA* is

rapidly dephosphorylated to form ppGpp, we refer to ppGpp for simplicity. Consistent with the opposing activities of RelA* and Mesh1*, the influence of either enzyme on exponential growth rate could be countered by the other in various growth media (Supplementary Fig. 1A, 1B). Hence, balanced ppGpp synthesis and hydrolysis yielded the stable ppGpp levels that allow for normal exponential growth of homogeneous cell populations (Supplementary Fig. 1C). A number of experiments were consistent. First, expression of the fluorescent proteins alone did not affect cell size or growth rate (Supplementary Fig. 1D-1G). Second, a strain unable to produce ppGpp ($ppGpp^0$, or *ΔrelA, ΔspoT*) did not grow in various minimal media lacking amino acids unless *relA** and *mesh1** were induced in a balanced manner (Supplementary Fig. 1B) [6, 30], in line with ppGpp activating amino acid biosynthesis operons [32, 33]. Third, in glucose rich medium containing amino acids, when ppGpp must be very low, Mesh1* induction did not affect growth (Supplementary Fig. 1H). Finally, we quantified ppGpp in wild-type *E. coli* (*relA*+ *spoT*+). These data confirmed that ppGpp levels indeed varied above and below normal concentrations when inducing *relA** or *mesh1** respectively (Fig. 1B).

ppGpp exerts cell size control

We studied the effects of ppGpp manipulation at the single-cell level using a microfluidic device that allowed media exchange, phase contrast and fluorescence microscopy, and cell-tracking algorithms[10, 34]. We determined the length at birth (L_B) and division (L_D), the cycle duration (T_{cyc}) and exponential growth or elongation rate (μ) for each cell cycle, and RelA* and Mesh1* enzyme concentrations, as quantified by the mean fluorescence per pixel (Fig. 1C, Supplementary Fig. 1C). We expressed either RelA* or Mesh1* at moderate levels in the wild-type background, to produce deviations in ppGpp relative to basal levels while maintaining balanced exponential growth (Fig. 1D-F).

As ppGpp decreased from above to below basal levels in glucose minimal medium, the (population-mean) trend in μ showed an optimum while L_B increased monotonically (Fig. 1D, E). The relation between L_B and μ (Fig. 1F) contained a number of intriguing features. First, as ppGpp decreased, both L_B and μ increased initially, in agreement with the well-known finding that faster growing cells are larger. However, decreasing ppGpp

further led to an inverted trend, in which slower growing cells are larger. This deviation began at near-endogenous ppGpp levels. A counter-intuitive consequence of this inversion is that excursions above and below this endogenous ppGpp level lead to cells that differ in size but grow equally fast (Fig. 1F, two example black dots on vertical line). The same trends were observed for the $ppGpp^0$ strain with RelA* and Mesh1* expression (Supplementary Fig. 2A).

The data are thus inconsistent with models in which ppGpp affects cell size by controlling growth. In such *hierarchical* models, L_B would follow the increase-optimum-decrease trend observed for μ (Fig. 1D). Instead, the monotonic increase of L_B with increasing ppGpp (Fig. 1E) suggested that ppGpp affects L_B in a way that is not mediated *via* μ. If ppGpp indeed modulates the size of cells in this manner, we surmised it should play a role in the adder mechanism, which maintains the cell size constant against stochastic variations in birth size.

ppGpp dynamically controls added cell size

In order to investigate the effect of ppGpp on the added size, we quantified the added length (ΔL) each cell cycle. First, we found that the adder principle was obeyed at all ppGpp concentrations: for the different levels of dox and IPTG induction, ΔL was birth-size independent (Fig. 2A). In line with previous adder principle observations, we find that T_{cyc} rather than μ is modulated to achieve a constant ΔL, as larger-born cells divide sooner (Fig. 2B). Indeed, ΔL increased monotonically with decreasing ppGpp (Supplementary Fig. 2B), and thus did not follow the trend observed for μ (Fig. 1D). These data indicated that the added size correlated with population-average ppGpp concentration rather than the rate of growth.

Next, we considered how shifts in ppGpp concentration affect cell size and its control dynamically. Within the microfluidic flow-cell, we followed individual cells as they were exposed to a shift from basal ppGpp concentrations to different levels of *relA** induction, in various growth media. First, the growth response underscored the important differences between moderate *relA** induction focused on here (1 and 2 ng/ml dox), and strong induction (10 ng/ml dox) that raises ppGpp to near-stringent response

concentrations [35]. The former allows continued exponential growth (Fig. 2C, D) while we find that the latter rapidly reduces μ and eventually arrests growth.

Notably however, the added size responded more rapidly than the growth rate, even for low *relA** induction levels. ΔL decreased halfway at about 25 min. and reached its final value at about 55 min. (Fig. 2C, red trace), while μ decreased halfway at about 100 min. and attained its final value at about 300 min. (Fig. 2C, blue trace). A similar pattern of rapid ΔL and slow μ responses were observed for different media and dox induction levels (Fig. 2E), as well as for *mesh1** induction (Fig. 2F). Consistently, ΔL increased more rapidly than μ decreased upon *mesh1** induction (Fig. 2F). Upon *relA** or *mesh1** induction, the cell width also decreased and increased respectively, albeit more slowly than for the added length (Supplementary Fig. 2C). We note that after reaching the final value, we found that ΔL can show an additional low-amplitude response component that is slower, in the form of a small undershoot and recovery after first reaching the final value at about 55 min (Fig. 2C). This slower variation was not seen in the majority of the conditions (Supplementary Fig. 3A). It suggested a fine-grained adaptation of the system, and may reflect an equilibration of other cellular processes in response to the ppGpp change that in turn affect ΔL.

The data show a temporal order in which ΔL responds to ppGpp deviations prior to μ. Indeed, ΔL typically has already reached its post-shift level when μ has decreased only half-way from pre-induction to post-induction level (Fig. 2D-F). These data support the idea that the effect of ppGpp on ΔL is not mediated by μ. We hypothesize that a change in ppGpp concentration sets a new added size by affecting the division frequency, which in turn results in a new steady-state birth size. Note that these observations do not imply that ppGpp control over size and growth are uncoupled. In addition to the effects observed here, there can be other processes that affect both the growth rate and division, including transcriptional control, altered metabolic conditions, stress or DNA damage.

Division accelerates transiently to achieve constant added size

We used mathematical modeling to understand the interplay between growth, division, and size, and compare different possible scenarios. Current size homeostasis models consider constant growth conditions, as well as a strict coupling between μ and

ΔL [1, 2, 36, 37]. We first tested a hierarchical model (Fig. 3A), which thus preserves the μ-ΔL coupling as growth conditions change. This model takes the observed initial and final values of μ and ΔL as input, lets μ decrease exponentially with the observed rate, and averages over multiple resulting simulated stochastic trajectories in ΔL and division frequency $1/T_{cyc}$. Note that while $1/T_{cyc}$ equals μ for exponentially growing populations in constant conditions, these quantities may not be strictly coupled when conditions change. The results of the hierarchical model (Fig. 3A) appeared inconsistent with the experimental observations (Fig. 3B). In particular, ΔL and μ decrease at similar rates in this model, while L_B decreases slower than μ (Fig. 3A), while the experiments show that both ΔL and L_B decrease faster than μ (Fig. 3B). Notably, the experimental data also indicate a transient increase in the division frequency $1/T_{cyc}$ before it decreases (Fig. 3B), unlike the hierarchical control model (Fig. 3A).

Next, we considered a model of *direct* ppGpp control, in which ppGpp changes also affect ΔL, but not via changes in μ (Fig. 3C). In this model, as also observed in the data (Fig. 2C), the mean ΔL responds directly by decreasing linearly to its post-shift value in about two pre-shift cell-cycles (note that division events in the averaged lineages are not synchronized), while μ decreases in the same way as in the previous model (Supplementary Fig. 3A). The direct control model reproduces many features of the experimental data. Specifically, L_B responds slower than ΔL but faster than μ, and $1/T_{cyc}$ showed a transient increase (Fig. 3B-F).

This increase in $1/T_{cyc}$ may appear paradoxical, as it must decrease ultimately to match the lower μ. However, with μ remaining comparatively high upon the shift, and ΔL decreasing faster, it is logical that divisions occur earlier as well. Nonetheless, the up and down modulation of the division frequency is notable. Together, these findings support the notion that the cells establish new targets for ΔL and L_B that are not set by the growth rate, and hence produce a transiently varying division frequency. Further observations are consistent with the direct model (Fig. 3D-H). First, $1/T_{cyc}$ changes on a timescale that is shorter than the cell cycle duration (28 minutes), or the C+D period (~65-75 minutes) [38]. When ppGpp shifts early in the cycle, the duration of that same cycle is reduced (from 28 to 22 mins, Fig. 3G, $p<10^{-3}$). Divisions occurred down to 15 min. after the shift, which provides a lower estimate of the response time. For shifts occurring mid-cycle or

late, it is logically the next (daughter) cycle that is reduced (Fig. 3H, $p<10^{-3}$). Thus, division can respond to ppGpp shifts within one cell cycle and depends on the timing of this shift within the cycle. Second, the direct model predicts that in minimal media, the $1/T_{cyc}$ changes would be much smaller compared to rich media and indeed may be too small to detect (Fig. 3F), owing to the lower μ. Third, upon Mesh1* induction, T_{cyc} increases within 25 minutes and then stays constant (Fig. 3I). These results indicate that ppGpp can exert control over division, and hence over cell size, in a way that is not mediated hierarchically through its effects on DNA replication initiation and the rate of growth. Experiments using a natural trigger of ppGpp synthesis supports this finding. Rapid amino acid starvation, which activates ppGpp synthesis by RelA in WT cells, led to multiple divisions and a population of small cells within 2 hours. In contrast, Δ*relA* cells divided at most once after the downshift and remained at a size similar to the pre-downshift average (Supplementary Fig. 3B).

Discussion

Elucidating the coordination between cell growth and cell cycle progression is a foundational challenge of microbial physiology. By directly manipulating ppGpp, we found that ppGpp is a cell division regulator, and hence serves as a link between growth and size control mechanisms. More specifically, we showed that *E. coli* cells do not follow a hierarchical model, in which cell size adjusts to the growth rate (as in the general growth law [7, 8, 13, 39], and ppGpp controls growth (by tuning ribosome production depending on amino acid availability, for instance). Rather, the (added) size correlates with the level of ppGpp (instead of the growth rate), and adjusts rapidly to ppGpp deviations, prior to the growth rate response. These observations indicate that ppGpp exerts control over cell division, in a way that is not mediated by the growth rate.

The findings lead to a number of speculations and implications. ppGpp is known to reflect diverse signals, including nutritional conditions, stress, biosynthetic activity, and metabolite availability [40, 41]. The proposed mechanism thus allows division control to integrate a wide spectrum of relevant growth factors. It may also help to accommodate physiological limitations. For instance, ribosome excess may require larger cells, but can incur a growth penalty due to metabolic costs, while the monotonic size-growth relation

of hierarchical models would impose smaller cells at lower growth. We indeed found that Mesh1* induction not only reduced growth (Fig. 1D), but also increased ribosome levels (Supplementary Fig. 3C) [30], which helps to explain the monotonicity deviation (Fig. 1F). These considerations are consistent with the idea that *E. coli* maximizes its growth rate rather than its size, and hence that size is modulated to accommodate associated requirements. Bacteria may deviate from the size-growth monotonicity also in other situations, with possible roles for ppGpp. Translation inhibitors can depress ppGpp and increase cell size [13, 42], overexpression of non-functional proteins can yield larger cells [43], while stochasticity can also cause monotonicity deviations (Supplementary Fig. 2A). Our results further indicate that ppGpp may serve to control recently observed division delays during nutrient up-shifts [44].

The growth changes observed here were slow compared to those triggered by ppGpp concentrations reached during the stringent response. Note that ppGpp increases can result in physiological effects that are slower than the immediate effects on its direct targets, such as RNA polymerases. For instance, ppGpp control of rRNA production can lead to lower ribosome levels by growth-mediated dilution on generation timescales. We found that division can respond within 20 minutes, which may reflect the time required to express divisome components, or to complete processes such as chromosome segregation and division ring assembly, which are regulated by nucleoid occlusion, the Min system, and other mechanisms [34, 45].

Diverse mechanisms have been proposed to explain cell size homeostasis and its dependence on growth [11-17]. Our findings suggest these mechanisms are under the control of ppGpp. For instance, the constant added size is proposed to result from the accumulation of a signaling molecule throughout the cell cycle, which triggers division when a threshold is exceeded [17]. One may speculate that ppGpp alters the production of this molecule and its threshold. Owing to the central role of ppGpp in metabolism and its many regulatory targets (hundreds of genes [46] and dozens of proteins [26, 47, 48]), ppGpp could control size in many possible ways. This may occur by transcriptional or post-transcriptional regulation, for instance of divisome proteins. It was found that OpgH can suppress FtsZ ring formation depending on the growth rate [49]. One may consider whether OpgH mediates the ppGpp division effects, though it is not a known ppGpp

interactor [26, 47, 48]. Nucleoid occlusion mechanisms have also been proposed to be involved in cell size regulation [1, 50]. Nucleoid volume could be modulated by ppGpp-induced decrease in the overall DNA replication initiation [27, 51] or transcription rates [52, 53].

In conclusion, our findings establish a link between ppGpp, the central signaling molecule in bacterial growth, and cell size homeostasis, which has implications for the diverse cellular components and processes that are involved in these two pivotal cellular control mechanisms.

Acknowledgements

We thank Mike Cashel for sharing *E. coli* CF10237. We thank Rebecca McKenzie, Martijn Wehrens, Nicole Imholz and Marek Noga for experimental assistance and helpful discussions throughout the project, Daan J. Kiviet for sharing his mold for the microfluidic device, and Flora Yang for assistance with LCMS measurements.

Author contributions

G.B., S.J.T., and F. B. conceived the experiments, F.B. performed the experiments, F. B., M.C.L. and J.G. performed the modelling, all authors contributed to the writing of the manuscript.

Declaration of interest

The authors declare no competing interests.

STAR Methods

Strains and plasmids

E. coli K-12 strains NCM3722 (CGSC# 12355) and ppGpp^0 (CF10237) which were transformed with a combination of *relA'-YFP* (*relA**), *mesh1-CFP* (*mesh1**) or *CFP* induction plasmids were used in all the experiments as described in the figures. Plasmid p*relA** was constructed by replacing mCherry on a pBbS2k-RFP plasmid (kanamycin

resistance, Tet promoter, sc101** origin) with a DNA sequence encoding the first 455 amino acids of the native *relA* gene (*relA'*). *YFP* fluorophore mVenus was fused to *relA'* via a glycine-serine linker using restriction cloning. Similarly, a codon optimized sequence of *mesh1** or *CFP* replaced mCherry in the plasmid pBbA5a-RFP (ampicillin resistance, lacUV5 promoter, p15A origin) leading to p*mesh1** and p*CFP*. p*mesh1** was built similarly to *relA** using restriction cloning to fuse *CFP* with *mesh1* via a glycine-serine linker. Further, immediately before the start codon of both genes a strong ribosomal binding site (AGGAGGAAAAAA) was added via SLiCE [54].

Chemocompotent NCM3722 cells were transformed with the p*relA** plasmid and spread on LB Agar plates with 25 ug/ml kanamycin. p*mesh1** and p*CFP* plasmids were transformed and plated on LB Agar plates with 50 ug/ml ampicillin. Plates older than 3 weeks were discarded and fresh transformations were prepared to prevent possible mutants.

Chemocompotent ppGpp^0 cells were co-transformed with p*relA** and p*mesh1** and plated on LB Agar plates with 50 µg/ml ampicillin, 25 µg/ml kanamycin and 100 µM IPTG to allow growth. Without 100 µM IPTG, leakage from p*relA** inhibits growth enough to prevent visible colonies next day morning (data not shown). Plates with colonies were only used on the day where the colonies first appear (next morning after transformation) as older plates loose viability rapidly.

Culture conditions

Cells for bulk and microscopy experiments were grown using defined MOPS medium containing 0.2% (with volume) carbon source (glucose, glycerol and malate) supplemented with 100 µM $MnCl_2$ (minimal media) [55]. Except Supplementary Figure 1B all of the experiments were conducted with glucose as the carbon source. Rich medium is the same as minimal media except for the supplementation of 0.2% Casamino acids, 400 µg/ml serine and 40 µg/ml tryptophan. 50 µg/ml ampicillin and 25 µg/ml kanamycin were added to the media along with appropriate plasmid bearing strains.

For ppGpp sampling experiments, cells were grown as described in Noga *et al*. [35]. Briefly cultures were inoculated from overnights into 250 ml Erlenmeyer flasks containing 25ml fresh media. Flasks were placed in a heated water bath set to 37˚C and mixed with a magnetic stirrer. MOPS glucose minimal media containing isotopically labelled $^{15}NH_4Cl$ was used in order to distinguish cellular ppGpp from unlabeled internal standard.

For the microscopy experiments, cells were initially inoculated in 10 mL tubes with 5 ml MOPS rich medium from a single colony in the morning. The tube was placed in a 37°C room on an orbital shaker until the growth becomes visible (OD ≈ 0.1). Cells were then spun down at 4000 G for 5 minutes and re-inoculated in 10 µL top media. 2 µL of the concentrated cells were injected into the microfluidic chip by hand via a p2.5 pipette and appropriate pipette tip.

$ppGpp^0$ strain requires different handling due to its inability to respond to stress. For the 96 well plate experiments, a single colony was inoculated in 5 ml glucose rich media with 100 µM IPTG and placed on a shaker for up to 4 hours until OD_{600} reaches 0.4. After that 40 ng/ml dox is added to prime the culture with high ppGpp production which allows it to handle stress and initiate growth in minimal media. This culture is then diluted in fresh media (MOPS minimal with different carbon sources) without any inducers. Immediately after the dilution, 98 µL of the culture is pipetted into wells of 96 well plates together with 1 µL dox and 1 µL IPTG (both at 100x final concentration), reaching a final volume of 100 µL. 96 well plates which were prepared as above were placed in a BioTek Synergy HTX plate reader maintained at 37 °C with constant orbital shaking. OD was measured every 10 minutes.

A similar method is applied for the microscopy experiments with the $ppGpp^0$ strain. A single colony is grown in rich media with proper antibiotics from the morning and when OD reached 0.1, 40 ng/ml dox is added to induce ppGpp production, which promotes cell survival during chip loading. The chip is then placed under the objective in a warm chamber set to 37°C for all the experiments. After cells populate the growth chamber input and output tubes are connected to the chip and appropriate media is pushed through

at 500 µl/hr. This corresponds to 250-500x dilution per hour since the chip's inner volume is between 1-2 µL.

Sample collection for ppGpp, DNA, and RNA quantification

Bulk cultures were induced with IPTG or dox at OD 0.1 (early exponential phase). Samples were taken either at OD 0.4 for growing cultures or 2.5 hours after maximum induction of RelA* (10 ng/ml). Rapid sample quenching, processing, and LCMS-based quantification of ppGpp were performed as described in Noga *et al.* [35].

RNA and DNA measurements were done using Quant-It RNA and Quant-IT DNA kits from InVitrogen-Molecular Probes and a BioTek Synergy HTX plate reader. Sampled volume was adjusted according to cell density (OD) as described in Potrykus et. al. [18].

Microfluidic flow cell

The microfluidic chip's Epoxy mold which was kindly sent by Daan J. Kiviet from Ackermann Lab is a variant of the mothermachine from Jun lab. Each flow line consists of an input which splits up into 2 arms, in each arm there are a number of extruding growth chambers varying in depth and width (80, 60, 40, 20, 10, 5 µm width, 60, 30, 50, 40 µm depth) and a single output after the 2 arms reconnect into a single line.

Chips were built by first preparing the PDMS mix using the protocol from the reference [15]. Polymer and curing agent (Sylgard 184 elastomer, Dow Corning) were prepared by mixing 7.7 g of polymer with 1mL of curing agent. The slight deviation from the suggested 10 g per 1 mL was implemented to create a more rigid chip allowing low height growth chambers to remain intact. Mixture was then thoroughly mixed using a vortexer and a plastic mixer. Then the mix was poured into the Epoxy mold (provided by Ackermann lab) and placed in a desiccator for 30 minutes to remove air bubbles formed during mixing. Then the mold is baked at 80°C for 1hr. After the baking period, the PDMS chip was removed from the mold using scalpels and rough edges were cut to allow for better binding to glass. Inlet and outlet holes were punched using a hole puncher. The PDMS chip was then covalently attached to a glass slide by using a hand-held corona treatment

device (model BD-20ACV, Electro-Technic Products). Application was done by passing the corona treatment device 6-7 times, each pass lasting ~5 seconds, 5-10 mm away from the surface of both the PDMS chip and glass cover slip. After the corona application, PDMS chips were placed on the treated glass surface and tapped by a gloved finger to assure full bonding. Prepared chips could be used couple weeks after preparation however after more than a month, chambers start to collapse, therefore chips older than 1 month were not often used.

Imaging and Image Analysis

Cells growing in the microfluidic chambers were imaged using an inverted Nikon TE2000. Using 100x and a 1.5x zoom lenses in tandem a pixel size of 0.041 μm was achieved. Imaging was done using a CMOS camera (Hamamatsu Orca Flash 4.0) via illumination from an LED light source (ImSpec, HPX-L5) with a liquid light guide. The microscope stance was equipped with a computer-controlled stage (Marzhauser, SCAN IM 120 3 100) allowing the stage to move between several chambers for imaging. A phase contrast image was taken every minute and a fluorescence image every 5 minutes using Chroma filter set 49003 and a computer-controlled shutter (Sutter, Lambda 10-3 with SmartShutter). Control of the automated microscopy systems was achieved through MetaMorph software. Each experiment lasts between 24-36 hours.

Images were initially visually checked for issues such as cells washing away from the wells or halting of growth due to clogs. After the initial checks, a MatLab based software customized by the Tans Lab was used to quantify growth rates and cell sizes. Individual cells were identified and tracked from phase contrast images. Cell's lengths and volumes were estimated assuming the shape of cylinders with semicircular caps and fitting a polynomial to skeletons of binary cell masks. Estimated length data through time was used to calculate instantaneous growth rate and average growth rate using exponential fits. Fluorescence values were calculated from a strip inside the cell area to decrease errors caused by fluorescence falloff that occurs at the edges of the cell. Added length was calculated by subtracting length at division (end of cycle) from length at birth (beginning of cycle). Duration of the cycles were calculated as the time between birth and

division. Width was calculated from the fitted cylinder. Any cell that did not divide within the growth chamber was ignored along with cells that approached the exits of the wells due to tracking issues caused by increased cell speeds near the exit.

Calculation of stabilization time

Data points within a sliding window of width ~T_{cyc} were compared against the data points where growth rate became stable after induction. As the sliding window moves through time (1 min steps), both growth rate and added length decrease and approach the final stable value. When the t-test between the data points in the sliding window and in the final stable growth regime yielded a p-value that exceeded 0.05 in three consecutive sliding time steps, the center of the window was defined as the “stabilization time”. For each experiment the data was randomly split into 3 parts and each part was analyzed using the same method (black dots, Figure 2D).

Division frequency analysis

Box plots (Figure 3D-F) were determined for measured values of $60/T_{cyc}$, in a period between 150 min. before induction and the moment of induction (green), and in a period between the moment of induction until two times the average pre-shift cell cycle time (blue).

Double normalization

In order to visually compare the changing rates of growth, division and cell size; a 2-sided normalization method was used. For each quantity, initial and final values were arbitrarily normalized to 2 and 1 respectively. Values of a and b were calculated such that [BeforeShiftAverage]*a+b = 2 and [AfterShiftAverage]*a+b = 1 from here the entire set of datapoints were normalized by [DataNorm.] = [Data]*a+b. This leads to vertical scaling of the data and allows visual comparison of different datasets. Since 2 and 1 were arbitrarily selected, when plotting, ‘Initial’ and ‘Final’ were chosen as labels for clarity.

Models

We considered two alternative models describing size control during the transient. In both models a cell divides with a hazard rate [21] that depends on the added size and a target added size ΔL (which in stationary conditions corresponds to the average added size). Both the target added size ΔL(t) and the growth rate μ(t) are functions of time during the transient. In both the models the growth rate μ(t) is exponentially relaxing to the stationary value observed in each of the experiments. The two models differ for the relation between growth rate and size scale during transient. In the hierarchical model, the typical size is a deterministic function of the growth rate (ΔL(t) = D*exp(μ(t)*T). Parameters were as follows: T = log(ΔLFinal/ΔLInitial)/(μFinal - μInitial) and D = ΔLInitial*exp(-μInitial*T). In the direct model, ΔL(t) is relaxing to the stationary value linearly in two pre-shift cycle duration time.

References

1. Campos, M., Surovtsev, I.V., Kato, S., Paintdakhi, A., Beltran, B., Ebmeier, S.E., and Jacobs-Wagner, C. (2014). A constant size extension drives bacterial cell size homeostasis. Cell *159*, 1433-1446.
2. Taheri-Araghi, S., Bradde, S., Sauls, J.T., Hill, N.S., Levin, P.A., Paulsson, J., Vergassola, M., and Jun, S. (2017). Cell-Size Control and Homeostasis in Bacteria. Curr Biol *27*, 1392.
3. Magnusson, L.U., Gummesson, B., Joksimovic, P., Farewell, A., and Nystrom, T. (2007). Identical, independent, and opposing roles of ppGpp and DksA in Escherichia coli. J Bacteriol *189*, 5193-5202.
4. Schreiber, G., Ron, E.Z., and Glaser, G. (1995). ppGpp-mediated regulation of DNA replication and cell division in Escherichia coli. Curr Microbiol *30*, 27-32.
5. Vadia, S., Tse, J.L., Lucena, R., Yang, Z., Kellogg, D.R., Wang, J.D., and Levin, P.A. (2017). Fatty Acid Availability Sets Cell Envelope Capacity and Dictates Microbial Cell Size. Curr Biol *27*, 1757-1767 e1755.
6. Xiao, H., Kalman, M., Ikehara, K., Zemel, S., Glaser, G., and Cashel, M. (1991). Residual guanosine 3',5'-bispyrophosphate synthetic activity of relA null mutants can be eliminated by spoT null mutations. J Biol Chem *266*, 5980-5990.
7. Pierucci, O. (1978). Dimensions of Escherichia coli at various growth rates: model for envelope growth. J Bacteriol *135*, 559-574.
8. Schaechter, M., Maaloe, O., and Kjeldgaard, N.O. (1958). Dependency on medium and temperature of cell size and chemical composition during balanced grown of Salmonella typhimurium. J Gen Microbiol *19*, 592-606.
9. Vadia, S., and Levin, P.A. (2017). Bacterial Size: Can't Escape the Long Arm of the Law. Curr Biol *27*, R339-R341.
10. Kiviet, D.J., Nghe, P., Walker, N., Boulineau, S., Sunderlikova, V., and Tans, S.J. (2014). Stochasticity of metabolism and growth at the single-cell level. Nature *514*, 376-379.

11. Cooper, S., and Helmstetter, C.E. (1968). Chromosome replication and the division cycle of Escherichia coli B/r. J Mol Biol *31*, 519-540.
12. Ho, P.Y., and Amir, A. (2015). Simultaneous regulation of cell size and chromosome replication in bacteria. Front Microbiol *6*, 662.
13. Si, F., Li, D., Cox, S.E., Sauls, J.T., Azizi, O., Sou, C., Schwartz, A.B., Erickstad, M.J., Jun, Y., Li, X., et al. (2017). Invariance of Initiation Mass and Predictability of Cell Size in Escherichia coli. Curr Biol *27*, 1278-1287.
14. Wallden, M., Fange, D., Lundius, E.G., Baltekin, O., and Elf, J. (2016). The Synchronization of Replication and Division Cycles in Individual E. coli Cells. Cell *166*, 729-739.
15. Witz, G., van Nimwegen, E., and Julou, T. (2019). Initiation of chromosome replication controls both division and replication cycles in E. coli through a double-adder mechanism. Elife *8*.
16. Harris, L.K., and Theriot, J.A. (2016). Relative Rates of Surface and Volume Synthesis Set Bacterial Cell Size. Cell *165*, 1479-1492.
17. Si, F., Le Treut, G., Sauls, J.T., Vadia, S., Levin, P.A., and Jun, S. (2019). Mechanistic Origin of Cell-Size Control and Homeostasis in Bacteria. Curr Biol *29*, 1760-1770 e1767.
18. Potrykus, K., Murphy, H., Philippe, N., and Cashel, M. (2011). ppGpp is the major source of growth rate control in E. coli. Environ Microbiol *13*, 563-575.
19. Cashel, M., and Gallant, J. (1969). Two compounds implicated in the function of the RC gene of Escherichia coli. Nature *221*, 838-841.
20. Ferullo, D.J., and Lovett, S.T. (2008). The stringent response and cell cycle arrest in Escherichia coli. PLoS Genet *4*, e1000300.
21. Jishage, M., Kvint, K., Shingler, V., and Nystrom, T. (2002). Regulation of sigma factor competition by the alarmone ppGpp. Genes Dev *16*, 1260-1270.
22. Traxler, M.F., Summers, S.M., Nguyen, H.T., Zacharia, V.M., Hightower, G.A., Smith, J.T., and Conway, T. (2008). The global, ppGpp-mediated stringent response to amino acid starvation in Escherichia coli. Mol Microbiol *68*, 1128-1148.
23. Vinella, D., Albrecht, C., Cashel, M., and D'Ari, R. (2005). Iron limitation induces SpoT-dependent accumulation of ppGpp in Escherichia coli. Mol Microbiol *56*, 958-970.
24. Seyfzadeh, M., Keener, J., and Nomura, M. (1993). spoT-dependent accumulation of guanosine tetraphosphate in response to fatty acid starvation in Escherichia coli. Proc Natl Acad Sci U S A *90*, 11004-11008.
25. Wang, B., Grant, R.A., and Laub, M.T. (2020). ppGpp Coordinates Nucleotide and Amino-Acid Synthesis in E. coli During Starvation. Mol Cell *80*, 29-42 e10.
26. Wang, B., Dai, P., Ding, D., Del Rosario, A., Grant, R.A., Pentelute, B.L., and Laub, M.T. (2019). Affinity-based capture and identification of protein effectors of the growth regulator ppGpp. Nat Chem Biol *15*, 141-150.
27. Kraemer, J.A., Sanderlin, A.G., and Laub, M.T. (2019). The Stringent Response Inhibits DNA Replication Initiation in E. coli by Modulating Supercoiling of oriC. mBio *10*.
28. Schreiber, G., Metzger, S., Aizenman, E., Roza, S., Cashel, M., and Glaser, G. (1991). Overexpression of the relA gene in Escherichia coli. J Biol Chem *266*, 3760-3767.
29. Gropp, M., Strausz, Y., Gross, M., and Glaser, G. (2001). Regulation of Escherichia coli RelA requires oligomerization of the C-terminal domain. J Bacteriol *183*, 570-579.

30. Zhu, M., and Dai, X. (2019). Growth suppression by altered (p)ppGpp levels results from non-optimal resource allocation in Escherichia coli. Nucleic Acids Res *47*, 4684-4693.
31. Sun, D., Lee, G., Lee, J.H., Kim, H.Y., Rhee, H.W., Park, S.Y., Kim, K.J., Kim, Y., Kim, B.Y., Hong, J.I., et al. (2010). A metazoan ortholog of SpoT hydrolyzes ppGpp and functions in starvation responses. Nat Struct Mol Biol *17*, 1188-1194.
32. Paul, B.J., Berkmen, M.B., and Gourse, R.L. (2005). DksA potentiates direct activation of amino acid promoters by ppGpp. Proc Natl Acad Sci U S A *102*, 7823-7828.
33. Paul, B.J., Barker, M.M., Ross, W., Schneider, D.A., Webb, C., Foster, J.W., and Gourse, R.L. (2004). DksA: a critical component of the transcription initiation machinery that potentiates the regulation of rRNA promoters by ppGpp and the initiating NTP. Cell *118*, 311-322.
34. Wehrens, M., Ershov, D., Rozendaal, R., Walker, N., Schultz, D., Kishony, R., Levin, P.A., and Tans, S.J. (2018). Size Laws and Division Ring Dynamics in Filamentous Escherichia coli cells. Curr Biol *28*, 972-979 e975.
35. Noga, M.J., Buke, F., van den Broek, N.J.F., Imholz, N.C.E., Scherer, N., Yang, F., and Bokinsky, G. (2020). Posttranslational Control of PlsB Is Sufficient To Coordinate Membrane Synthesis with Growth in Escherichia coli. mBio *11*.
36. Osella, M., Nugent, E., and Cosentino Lagomarsino, M. (2014). Concerted control of Escherichia coli cell division. Proc Natl Acad Sci U S A *111*, 3431-3435.
37. Ho, P.Y., Lin, J., and Amir, A. (2018). Modeling Cell Size Regulation: From Single-Cell-Level Statistics to Molecular Mechanisms and Population-Level Effects. Annu Rev Biophys *47*, 251-271.
38. Bremer, H., and Dennis, P.P. (2008). Modulation of Chemical Composition and Other Parameters of the Cell at Different Exponential Growth Rates. EcoSal Plus *3*.
39. Vadia, S., and Levin, P.A. (2015). Growth rate and cell size: a re-examination of the growth law. Curr Opin Microbiol *24*, 96-103.
40. Hauryliuk, V., Atkinson, G.C., Murakami, K.S., Tenson, T., and Gerdes, K. (2015). Recent functional insights into the role of (p)ppGpp in bacterial physiology. Nat Rev Microbiol *13*, 298-309.
41. Ronneau, S., and Hallez, R. (2019). Make and break the alarmone: regulation of (p)ppGpp synthetase/hydrolase enzymes in bacteria. FEMS Microbiol Rev *43*, 389-400.
42. Baracchini, E., and Bremer, H. (1988). Stringent and growth control of rRNA synthesis in Escherichia coli are both mediated by ppGpp. J Biol Chem *263*, 2597-2602.
43. Basan, M., Zhu, M., Dai, X., Warren, M., Sevin, D., Wang, Y.P., and Hwa, T. (2015). Inflating bacterial cells by increased protein synthesis. Mol Syst Biol *11*, 836.
44. Panlilio, M., Grilli, J., Tallarico, G., Iuliani, I., Sclavi, B., Cicuta, P., and Lagomarsino, M.C. (2020). Threshold accumulation of a constitutive protein explains E. coli cell division behavior in nutrient upshifts. bioRxiv, 2020.2008.2003.233908.
45. Arjes, H.A., Kriel, A., Sorto, N.A., Shaw, J.T., Wang, J.D., and Levin, P.A. (2014). Failsafe mechanisms couple division and DNA replication in bacteria. Curr Biol *24*, 2149-2155.
46. Liu, K., Bittner, A.N., and Wang, J.D. (2015). Diversity in (p)ppGpp metabolism and effectors. Curr Opin Microbiol *24*, 72-79.
47. Kanjee, U., Ogata, K., and Houry, W.A. (2012). Direct binding targets of the stringent response alarmone (p)ppGpp. Mol Microbiol *85*, 1029-1043.

48. Zhang, Y., Zbornikova, E., Rejman, D., and Gerdes, K. (2018). Novel (p)ppGpp Binding and Metabolizing Proteins of Escherichia coli. mBio *9*.
49. Hill, N.S., Buske, P.J., Shi, Y., and Levin, P.A. (2013). A moonlighting enzyme links Escherichia coli cell size with central metabolism. PLoS Genet *9*, e1003663.
50. Wu, L.J., and Errington, J. (2011). Nucleoid occlusion and bacterial cell division. Nat Rev Microbiol *10*, 8-12.
51. Fernandez-Coll, L., Maciag-Dorszynska, M., Tailor, K., Vadia, S., Levin, P.A., Szalewska-Palasz, A., and Cashel, M. (2020). The Absence of (p)ppGpp Renders Initiation of Escherichia coli Chromosomal DNA Synthesis Independent of Growth Rates. mBio *11*.
52. Jin, D.J., and Cabrera, J.E. (2006). Coupling the distribution of RNA polymerase to global gene regulation and the dynamic structure of the bacterial nucleoid in Escherichia coli. J Struct Biol *156*, 284-291.
53. Hadizadeh Yazdi, N., Guet, C.C., Johnson, R.C., and Marko, J.F. (2012). Variation of the folding and dynamics of the Escherichia coli chromosome with growth conditions. Mol Microbiol *86*, 1318-1333.
54. Motohashi, K. (2017). Seamless Ligation Cloning Extract (SLiCE) Method Using Cell Lysates from Laboratory Escherichia coli Strains and its Application to SLiP Site-Directed Mutagenesis. Methods Mol Biol *1498*, 349-357.
55. Neidhardt, F.C., Bloch, P.L., and Smith, D.F. (1974). Culture medium for enterobacteria. J Bacteriol *119*, 736-747.

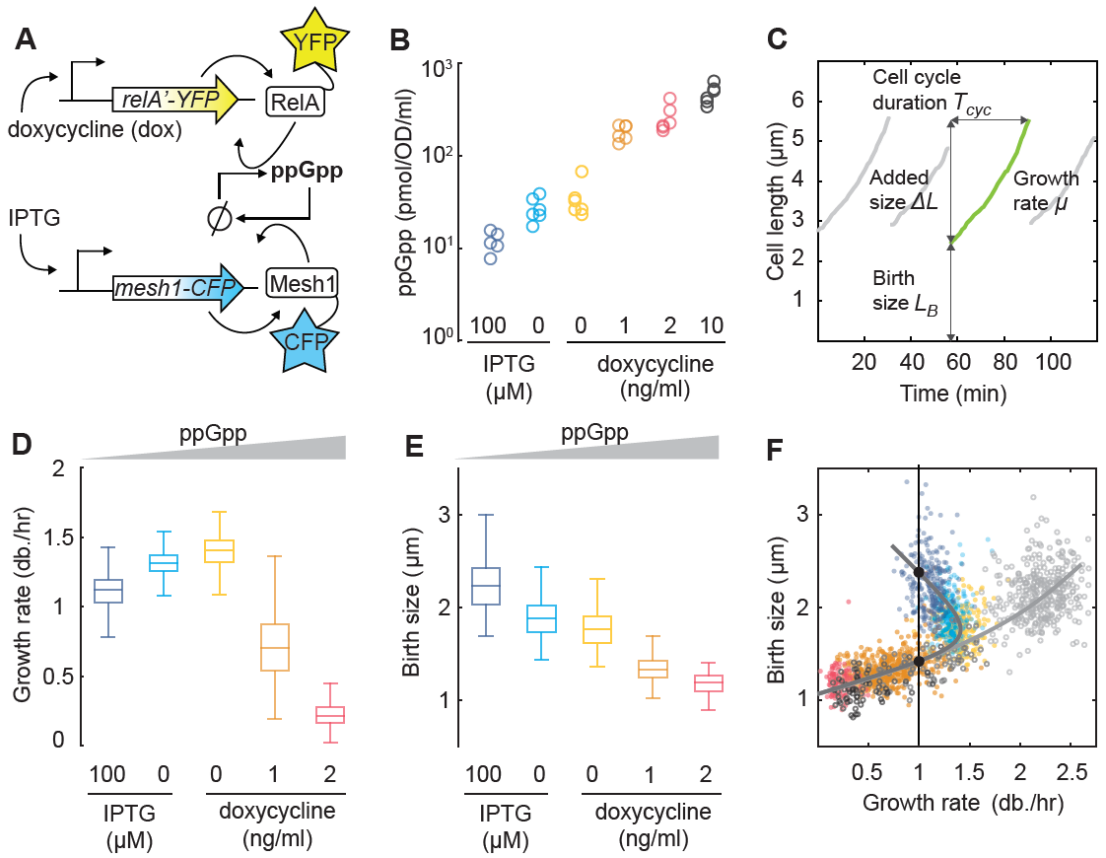

Figure 1. ppGpp exerts cell size control. (A) Scheme to control the ppGpp concentration. *E. coli* RelA truncate (*relA'*), fused to YFP, is induced by dox, which leads to ppGpp via synthesis and dephosphorylation of pppGpp (not shown). The ppGpp hydrolysis enzyme Mesh1, fused to CFP, is induced by IPTG. **(B)** Intracellular ppGpp concentrations after induction of *mesh1-CFP* (*mesh1** from here) or *relA'-YFP* (*relA** from here) compared to basal levels, in glucose minimal medium. Shown are 2-3 measurements from two biological replicates. **(C)** Measured cell length for a single lineage, as grown in a microfluidic device. For each cell cycle we quantified size (length) at birth (L_B), cell cycle duration (T_{cyc}), added size (ΔL), and the growth rate (μ) by exponential fitting. **(D)** Growth rate for increasing ppGpp levels in glucose minimal medium (left to right, see panel B). Left to right: N = 270, 254, 255, 479, 119 cell cycles. μ peaks at basal ppGpp levels (no induction), and then decreases. **(E)** Birth size for increasing ppGpp levels. Conditions as in panel B. L_B increases continuously, while μ decreases for below-basal ppGpp levels. **(F)** Birth length against growth rate. Closed circles: single cell cycles in minimal media, colors and conditions as in panel B. Drawn curves are guides to the eye. Notably, for below-basal ppGpp, slower growing cells are larger, owing to an inversion of the growth law. Cells of different size can thus have the same growth rate (black dots). Open circles: single cell cycles in glucose rich media including amino acids, with 2 ng/ml, 1 ng/ml, or 0 ng/ml dox, and N = 70, 68, 340 cell cycles (dark to light gray).

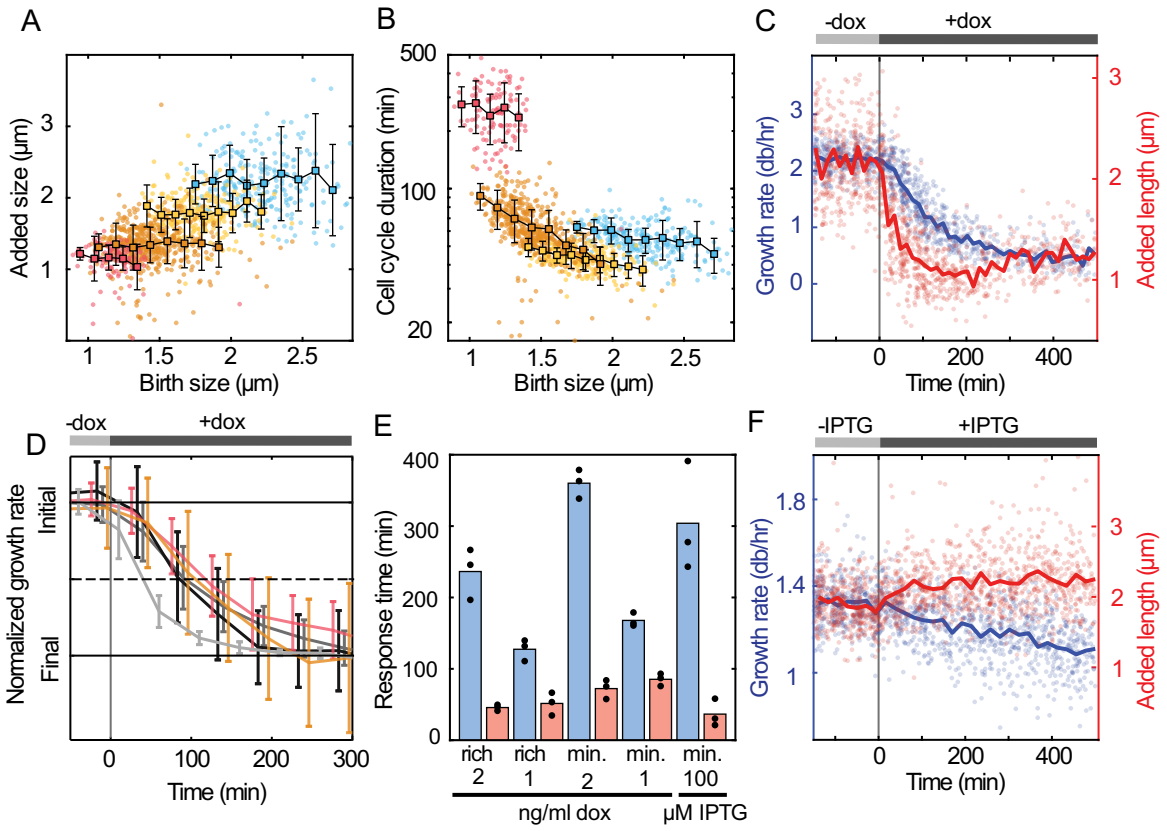

Figure 2. ppGpp dynamically controls added cell size. (A) Cell length added per cell cycle (ΔL) against birth length (L_B) of that cycle, for different constant ppGpp levels. Dots are single cell cycles, squares are means for L_B bin, bars are s.e. Left to right: clouds for decreasing ppGpp levels, starting with dox in ng/ml: 2 (red), 1 (orange), 0 (yellow), and 100 μM IPTG (blue). N = 119, 479, 255, 270 cell cycles. For each cloud, ΔL is constant for different L_B, consistent with the adder principle. **(B)** Cell cycle duration (T_{cyc}) against birth length (L_B) of that cycle. Within a cloud, when L_B is smaller, T_{cyc} is typically larger on average, indicating it is modulated as cells compensate for stochastic variations in L_B, which is consistent with the adder principle. Colors and conditions as in panel A. **(C)** Growth rate (μ) and added size (ΔL) during a ppGpp increase. Circles are single cell cycles, lines are moving averages, for a shift from 0 to 2 ng/ml dox, in rich glucose medium. ΔL responds faster than μ and reaches the post-shift value while μ decreases. **(D)** Growth rate (μ) during different ppGpp increases (*relA** induction for different dox concentrations), in glucose rich and minimal media. μ response timescale for these various conditions is assessed by normalizing rate to initial (pre-shift) and final (post-shift) value. Top bar indicates dox induction. In minimal media, shift from 0 ng/ml dox to: 2 (pink), and 1 (orange). In rich media, shift from 0 ng/ml dox to: 1 (dark gray), 2 (intermediate gray), and 10 (light gray). Bars are s.e.m. For moderate (1 and 2 ng/ml) shifts, the adaptation time is similar and growth remains exponential. For the larger 10 ng/ml shift, the growth decreases faster and arrests after the shift, in line with ppGpp approaching stringent response levels. **(E)** Response time for μ (blue) and ΔL (red) (see methods). Black dots represent one third of the data points. ΔL responds faster than μ under all moderate shifts. **(F)** Growth (μ) and added size (ΔL) during a ppGpp decrease. Circles are single cell cycles, lines are moving averages, for shift from 0 to 100 μM IPTG, in glucose minimal medium. For the resulting below-basal ppGpp levels, the added cell size increases while growth rate decreases.

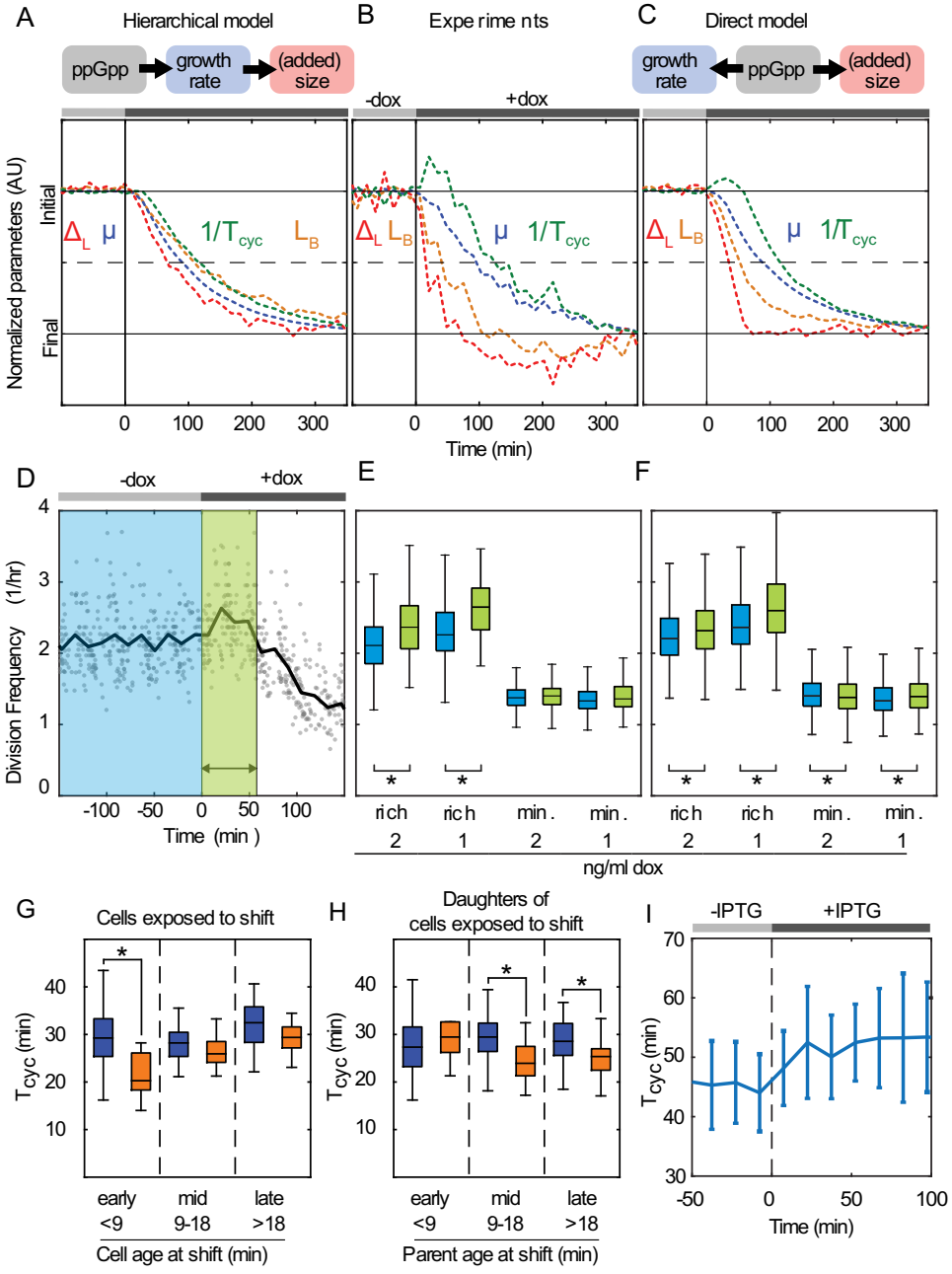

Figure 3 Division accelerates transiently to achieve constant added size. (A) Predictions of hierarchical model, in which ppGpp affects the growth rate (μ), and in turn added size adjusts to the growth rate. To compare response speeds, indicated quantities are normalized to initial (pre-shift) and final (post-shift) values. Top bar indicates ppGpp increase. **(B)** Experimental data. Conditions as in panel A. **(C)** Predictions of direct model, in which ppGpp exerts control over division and hence (added) size, without being mediated by μ. Conditions as in panel A. The data agrees with direct model, both in terms of the temporal order of the responses, and the transient acceleration of divisions. **(D)** Quantification of transient effects in the division frequency ($1/T_{cyc}$). Data is averaged in purple and green (width equals $2*T_{cyc}$, black arrow) zones to produce data in panels E and F. Circles are single cell cycles for shift from 0 to 2 ng/ml dox, in glucose minimal

medium. Drawn line is moving average. **(E)** Experimental pre- and post-shift division frequency ($1/T_{cyc}$), as defined in panel D. In rich media, up to a ~15% increase is observed between. Star: $p < 0.01$. (N = 340, 187, 98, 62, 255, 193, 226, 220 left to right) **(F)** Direct model yields transient changes for 1/Tcyc. Star: p<0.01. Note the model detects small changes due to high number of cells used (5000 pre-shift, 3000 post-shift). **(G)** Measured cell cycle duration (T_{cyc}) during ppGpp up shift (2 ng/ml dox, rich media, orange) compared to cells before the shift (between -140 and -90 min., blue). Cells that are young (<9 min. after birth) during shift show decreased T_{cyc} in the same cycle as the shift. N=61, 11, 28, 23, 51, 33. Star: $p<10^{-3}$. **(H)** T_{cyc} of the progeny of the cells in panel G (orange), showing decreases when the ppGpp shift occurs mid-cycle and late in their parent. N = 73, 6, 22, 25, 48, 43. Star and blue box plots as in panel G. **(I)** Cell cycle duration during ppGpp down-shift. Induction of *mesh1** (T=0 mins) leads to increase in T_{cyc} within one cell cycle, suggesting inhibition of division by decreased ppGpp levels.

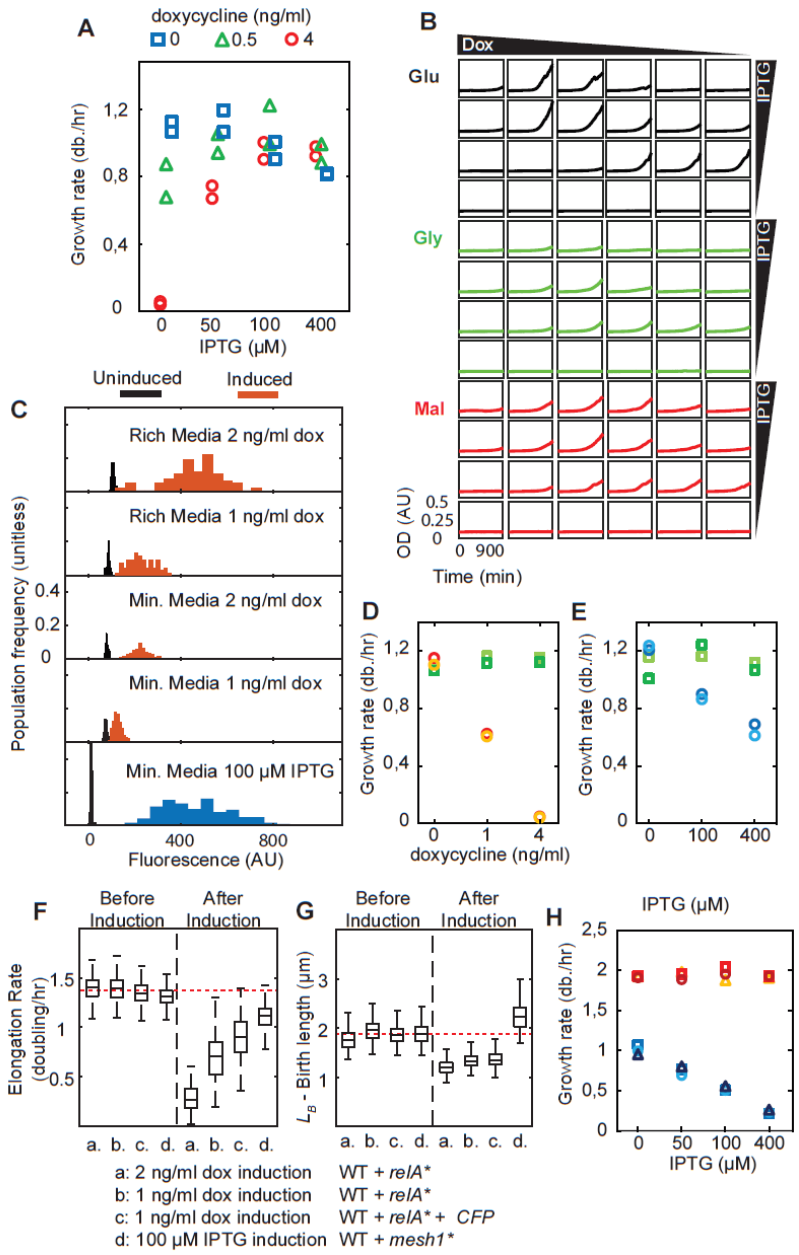

Supplementary Figure 1: Expression, growth, and size characterization. (A) Growth rate of *WT* strain (*relA+ spoT+)* including *relA** and *mesh1** plasmids, for different dox and IPTG levels, in minimal glucose media. At high dox (red), increased IPTG yields increased growth rate, consistent with Mesh1 decreasing the ppGpp level. Medium dox (green triangles) yield optimum growth for intermediate IPTG. Without dox (blue squares), *mesh1** induction yields decreased growth beyond 100 μM IPTG. **(B)** Optical density (OD) in time for $ppGpp^0$ (*ΔrelA, ΔspoT*) strain including *relA** and *mesh1** plasmids, in minimal media (black: glucose, green: glycerol, red: malate). Without *mesh1** induction by IPTG no growth is detected, consistent with lethal ppGpp accumulation. Similarly, growth is minimal with maximal *mesh1** and no *relA** induction (top right plots), as minimal ppGpp arrests growth in minimal media. Growth effects of the enzymes can be compensated for by the other enzyme: the top-left to bottom-right plots display the fastest growth. This data is consistent with RelA' synthesizing ppGpp, and Mesh1* hydrolyzing it. **(C)** Cellular

fluorescence, showing homogeneous induction in the population. Conditions as indicated. Y axes are identical in all plots**.** Data taken before and after induction of *relA** with 1 or 2 ng/ml dox or *mesh1** with 100 μM IPTG. Details as in Fig. 1B, D-F **(D)** Population growth rate upon induction of *YFP* only (green and lime squares), *relA** (orange and red circles), in duplicate, in glucose minimal media, showing YFP expression alone does not affect the growth rate. **(E)** Population growth rate upon induction of *CFP* only (green and lime squares), and *mesh1** (blue and cyan circles) in duplicates, indicating *CFP* induction alone does not reduce the growth rate. **(F, G)** Growth rates and birth sizes for different strains and shifts. Strains are as indicated. Medium is glucose minimal. Cellular growth rates (panel F) and birth lengths (panel G) were quantified before (left) and after (right) the indicated induction. Condition *c*: *CFP* was continuously induced with 200 μM IPTG. Consistently, this *CFP* induction yields similar growth rates and cell sizes as without it (F and G, c-left and b-left, respectively). Upon induction of *relA** (dox) or *mesh1** (IPTG) all the strains grow slower (F, right vs left). Induction of *mesh1** increases cell size (G, d-right vs d-left), indicating the size effect is caused by *mesh1** rather than *CFP* alone. 2 ng dox induction decreases the growth rate to ~0.25 db/hr (F, a-right). Consistently, 1 ng dox induction leads to a higher final growth rate (F, b-right and c-right). Red dotted horizontal line is average of 4 experiments before induction of *relA** or *mesh1**. Number of cell cycles measured: N=255, 159, 223, 254, 119, 479, 392, 270 left to right (panels F and G). **(H)** Induction of *mesh1** in rich (filled symbols) and minimal (empty symbols) MOPS glucose media. In rich media the growth rate is unaffected by *mesh1** induction because ppGpp is not required for growth.

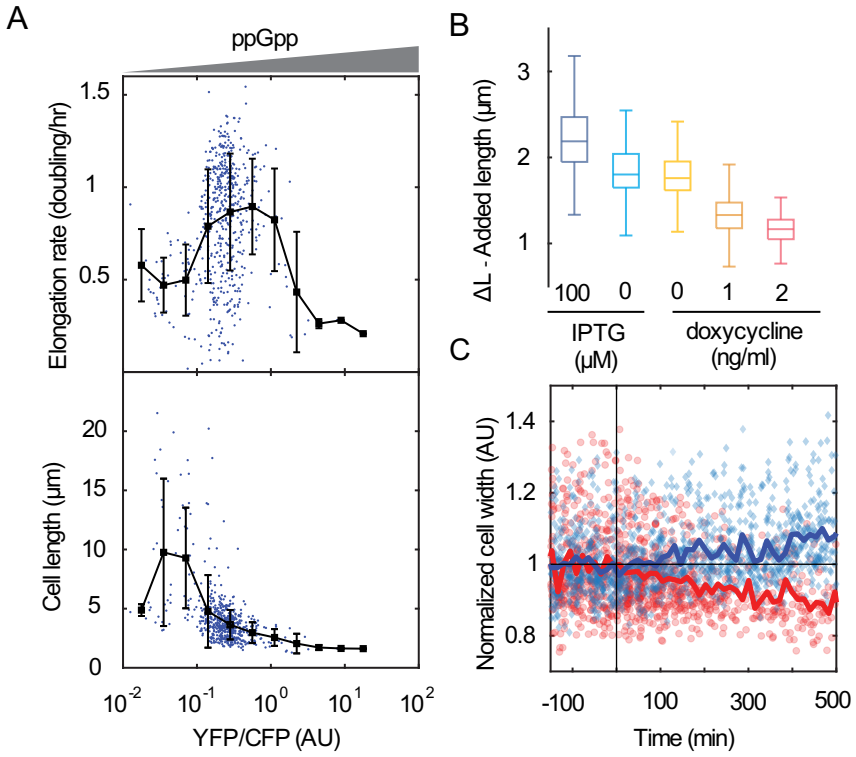

Supplementary Figure 2: Effects of *relA and *mesh1** induction. (A)** Cellular growth rates (top) and birth lengths (bottom) against ppGpp level, quantified by YFP/CFP, for a $ppGpp^0$ strain with *relA'** and *mesh1** plasmids, in minimal glucose media. Detected variation along YFP/CFP axis indicates stochasticity of *relA** and *mesh1** expression. Growth shows peak for increasing YFP/CFP, while the (birth) size decreases systematically. These results support similar findings in Fig. 1D-F. N = 563 cells. **(B)** Added length for increasing ppGpp levels in glucose rich medium (see Fig. 1B). Conditions and number of cell cycles as in Fig. 1D-F. ΔL decreases systematically with increasing ppGpp levels, rather than following the growth rate trend, which instead peaks with ppGpp (Fig. 1D). **(C)** Width of cells undergoing *relA** induction (2 ng/ml dox) in glucose rich media (red circles) or *mesh1** induction (100 μM IPTG) in minimal media (blue diamonds). Induction is at 0 min. Data is normalized to the average width before induction. Lines are average trends. The cell widths change in the same direction as the length (Fig. 2), at a slower timescale. (*relA** red N=1043, *mesh1** blue N=1285 cell cycles)

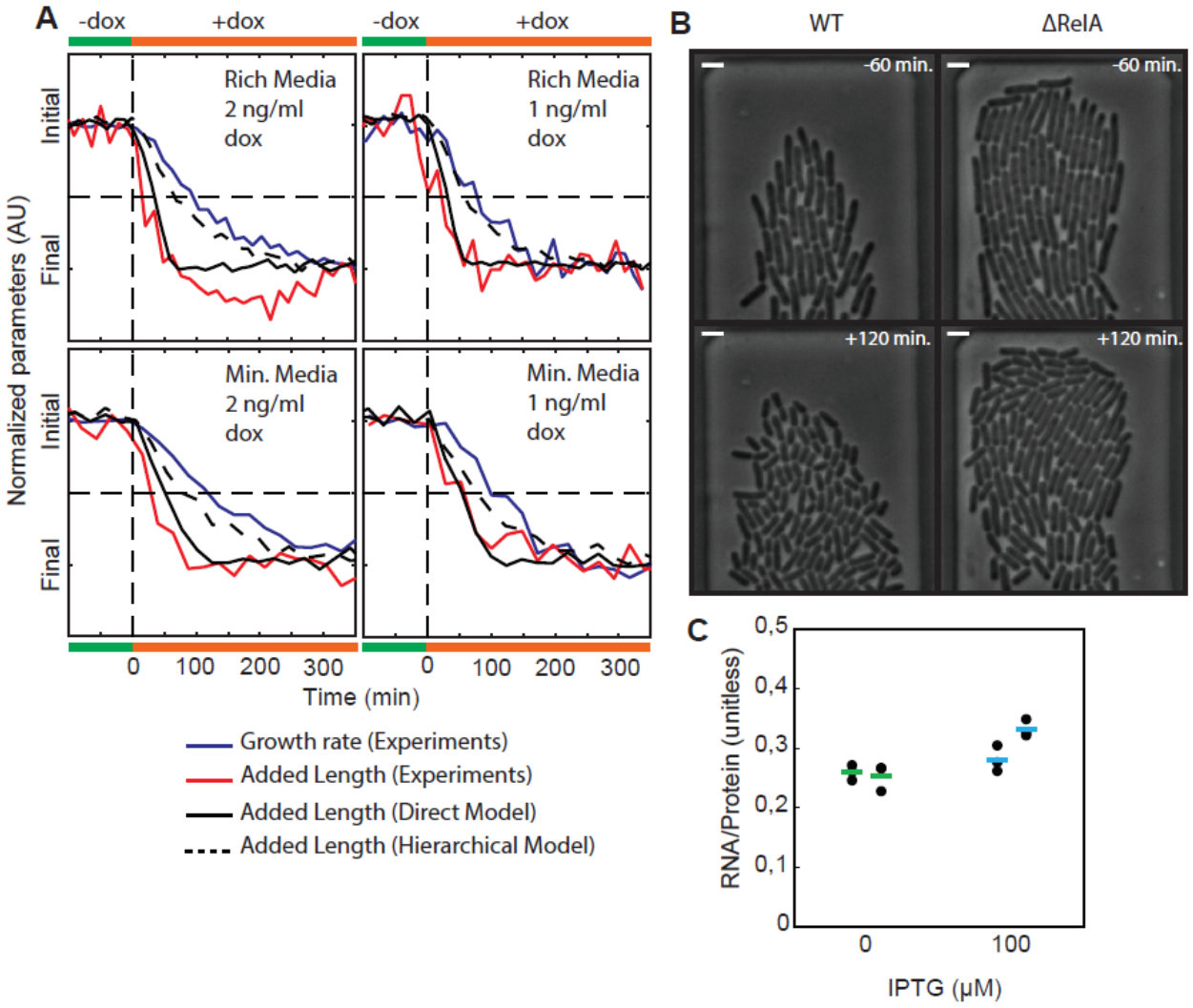

Supplemental Figure 3. Cell cycle parameters during ppGpp shifts. (A) Normalized cellular growth rate and added length during ppGpp shifts. A strain carrying *relA** plasmid was grown in rich (with amino acids) or minimal (without amino acids) glucose MOPS media. Induction of *relA** with 2 or 1 ng/ml dox occurs at t = 0 mins (vertical dashed line). Indicated are moving averages of the growth rate (blue) and added length (red) from experiments and computed added length from two models (solid black: direct model, dashed black: hierarchical model). indicated quantities are normalized to initial (pre-shift) and final (post-shift) values. Horizontal dashed lines are half-way between initial and final values. The hierarchical adder model does not follow the experimentally observed ΔL trajectory (red curve), while the direct adder model does. **(B)** Images of *WT* and *ΔrelA* strains 1 hour before and 2 hours after a downshift from MOPS glucose rich (with amino acids) to MOPS glucose media (without amino acids). Before the shift the cells are of similar size. Upon the shift the *ΔrelA* cells do not divide as rapidly as the WT cells, and hence are larger. The data indicate that ppGpp has an effect on the division frequency, consistent with our other findings. White bar represents 1 μm. **(C)** Effect of *mesh1** induction on RNA/protein ratio (from 0.26 to 0.31 p=0.0017), which reflects the concentration of ribosomes. Induction of *mesh1** with 100 μM IPTG yields lower than basal ppGpp levels (Fig. 1B).